



TITLE:

# Scaled dynamic loading tests on seismic isolation bearing excluding the contamination of friction and inertia forces

AUTHOR(S):

Takeuchi, Toru; Takahashi, Yoshikazu; Umemura, Yukio; Terazawa, Yuki; Uemura, Keita; Ueda, Tomoya

---

CITATION:

Takeuchi, Toru ...[et al]. Scaled dynamic loading tests on seismic isolation bearing excluding the contamination of friction and inertia forces. *Engineering Structures* 2023, 296: 116844.

ISSUE DATE:

2023-12-01

URL:

<http://hdl.handle.net/2433/285546>

RIGHT:

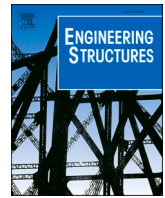
© 2023 The Author(s). Published by Elsevier Ltd.; This is an open access article under the CC BY license.



Contents lists available at [ScienceDirect](https://www.sciencedirect.com)

Engineering Structures

journal homepage: [www.elsevier.com/locate/engstruct](http://www.elsevier.com/locate/engstruct)



## Scaled dynamic loading tests on seismic isolation bearing excluding the contamination of friction and inertia forces

Toru Takeuchi<sup>a,\*</sup>, Yoshikazu Takahashi<sup>b</sup>, Yukio Umemura<sup>a</sup>, Yuki Terazawa<sup>a</sup>, Keita Uemura<sup>b</sup>, Tomoya Ueda<sup>b</sup>

<sup>a</sup> Tokyo Institute of Technology, Department of Architecture and Building Engineering, Ookayama 2-12-1, Meguro-ku, Tokyo 152-8550, Japan

<sup>b</sup> Kyoto University, Department of Civil and Earth Resources Engineering, Nishikyo-ku, Kyoto 615-8540, Japan

### ARTICLE INFO

#### Keywords:

Seismic isolation  
Bearing  
Dynamic test  
Friction  
Inertia force  
Hybrid simulation

### ABSTRACT

Conventional seismic isolation-bearing testing facilities require moving horizontal platens under high compression. However, these dynamic moving platens inevitably lead to the friction and inertial forces generated by large vertical loads and inertial forces due to the dynamic mass action of the moving platen, which eventually affects the accuracy of the measured force. To solve this problem, the authors have proposed a direct reaction force measurement system (horizontal-vertical separated type) that can exclude the contamination of friction and inertial forces. Measuring pure reaction forces without the contamination of friction forces and inertia is crucial for the reliability of test results. In this paper, prior to the construction of large-scale facility, reduced-size-mockup dynamic tests were conducted using the proposed measurement concept, and its validity and accuracy were discussed. Furthermore, this system was applied to hybrid simulation tests, and the significant improvement of the proposed measurement system was observed.

### 1. Introduction

Seismic isolated buildings supported by seismic isolation bearings can significantly reduce the response of structures to earthquakes if properly designed, and the number of such applications in Japan alone has exceeded 5,200 buildings by 2023. Seismic isolation is beginning to be used not only in high-rise buildings but also in large bridges that support transportation infrastructure.

Among the typical rubber bearings used for seismic isolation, natural rubber-based laminated rubber bearings have a relatively linear stress-strain relationship, while lead-plugged rubber bearings, high-damping rubber bearings, and friction-type bearings with additional damping functions are known to exhibit complex behavior under high axial forces and large dynamic deformations, and also depend on the size of the bearing. Their dependencies have been researched in major test facilities such as MCEER [1,2], etc., and it is known that lead-plugged rubber bearings have high pressure dependencies and high-damping rubber bearings have pressure, temperature, and frequency dependencies. The numerical modeling of these bearings is complicated due to their size, velocity, pressure, and temperature dependence. Therefore, it is very important to verify the behavior of seismic isolation

bearings using full-scale dynamic test facilities. However, no facility in Japan can dynamically test full-scale bearings larger than 800 mm in diameter, such as those used in large scale buildings and bridges, and such performance tests have been relied upon at testing facilities outside Japan, such as in the United States and Taiwan [3,4]. Fig. 1(a) shows the Seismic Response Modification Device (SRMD) test facility at UCSD. The moving platen that shears the specimen is moved dynamically in the horizontal direction while being subjected to upward vertical forces of tens of thousands of kilonewtons. However, the frictional forces caused by the large vertical force and inertial force of the heavy platen are mixed into the measured reaction force of the load cell attached to the horizontal dynamic jack. Alireza *et al.* [5] conducted a real-time hybrid simulation experiment to correct the inertial force by measuring the acceleration and constructing an accurate friction model for the frictional force. Also, friction models considering the effects of velocity and pressure have been proposed and provided in OpenSees based on the studies such as [1,6]. However, it is still not easy to accurately reproduce a complex friction model that depends on the individual test machine conditions, and the time delay involved in the calculation is a challenge for real-time hybrid simulation experiments.

In a previous report [7], the authors have proposed a new type of

\* Corresponding author.

E-mail address: [takeuchi.t.ab@m.titech.ac.jp](mailto:takeuchi.t.ab@m.titech.ac.jp) (T. Takeuchi).

<https://doi.org/10.1016/j.engstruct.2023.116844>

Received 4 April 2023; Received in revised form 23 August 2023; Accepted 30 August 2023

Available online 25 September 2023

0141-0296/© 2023 The Author(s). Published by Elsevier Ltd. This is an open access article under the CC BY license (<http://creativecommons.org/licenses/by/4.0/>).

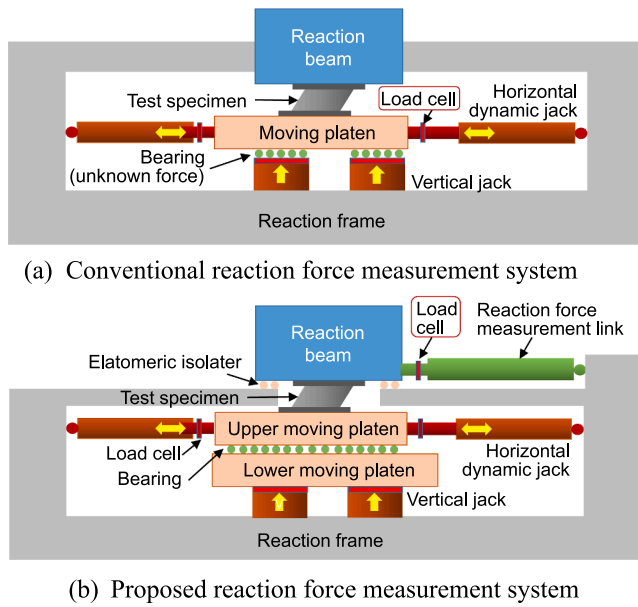


Fig. 1. Conventional and proposed measurement system.

reaction force measurement system, as shown in Fig. 1(b), where a reaction beam was placed on top of the specimen, which was elastically supported with very low stiffness in the horizontal direction and almost rigid in the vertical direction, and the rigid reaction force measurement links were connected to the reaction beam in the horizontal direction. Most of the horizontal reaction force was measured in real-time using these force measurement links, and because the reaction beam hardly moved, almost no inertial force was generated. Furthermore, by supporting the reaction beam with elastomeric isolators, which are soft in the horizontal direction and rigid in the vertical direction, only 1–2% of the horizontal force transmitted through these elastomeric isolators can be accurately calculated by their measured deformation. The method of eliminating frictional and inertial forces by simultaneously measuring compressive and shear forces inserting 3D load-cells between the reaction beam and specimen has already been introduced in several reports [2,8] with limited test results. However, in order to withstand vertical forces of several thousand tones, dozens of 3D load-cells have to be arranged and the axial and shear forces calculated from the combined forces, which not only requires handling a large amount of data but also introduces errors due to the correlation between axial and shear forces. The required shear force is roughly 10% of vertical load in typical seismic isolation testing systems, therefore, shear strain on a rigid load cell that can withstand high axial force will be negligible, especially in smaller specimens, making it difficult to ensure accuracy. In the method proposed by authors, the horizontal and vertical reaction forces are separated, a small numbers of large-capacity load cells with single axis are placed in each direction, thereby simplifying and increasing the reliability of the data handled. However, the effectiveness of the proposed type of measurement system and its validation under dynamic experiments have not yet been confirmed.

Therefore, prior to the construction of the full-scale test facility, a scaled-down-mockup test apparatus that incorporated the proposed measurement system was constructed and validity of the proposed system is confirmed focusing on the horizontal reaction forces. Dynamic-loading tests were conducted on laminated rubber-bearing specimens with different rubber hardness subjected to a vertical force. Through these experiments, the reaction force values obtained using the conventional load cell on the dynamic jack subjected to the inertial and frictional forces of the moving platen were compared, and the efficiency of the proposed measurement system was investigated. In addition, a hybrid simulation test was conducted using the proposed apparatus,

linking a laminated rubber-bearing specimen and a virtual multistory building to analyze the effect of the difference in the measurement system on the response results.

## 2. Reduced-scale mock-up experiment

To verify that the proposed reaction force measurement system works in practice, dynamic-loading experiments were performed using a reduced-scale setup. This section presents the experimental setup, measurement plan, and loading plan for the mockup experiment.

### 2.1 Experimental setup

#### 2.1.1. Configuration of the experimental setup

The experiment was conducted using a dynamic test frame located at the Tokyo Institute of Technology Midorigaoka Campus. The test setup is shown in Fig. 2. This test frame was equipped with a horizontal dynamic jack that could be loaded in one direction and a moving platen supported by two linear sliders. The horizontal dynamic jack had a maximum load of 500 kN, maximum velocity of 500 mm/s, and maximum positive and negative amplitudes of  $\pm 300$  mm. Because there was no existing vertical-loading device in this frame, it was newly installed in the test set-up.

The plan, sectional, and exploded views are presented in Fig. 3. The test set-up consists of, from bottom to top, a moving platen, the specimen, a vertical force apparatus, and a reaction beam. V-shaped horizontal reaction force measurement links with the load cells were attached to the side of the reaction beam, and the reaction beam was supported by elastomeric isolators (laminated natural rubber bearings) attached to the bottom beam. The reaction beam was tightly connected to the bottom beam by eight PC-steel rods, and the initial applied tension exceeded 1600 kN so that the elastomeric isolators supporting the reaction beam will not lift up. The ends of the PC-steel rods were anchored using rotational nuts and remained horizontally movable. These configurations are equivalent to those of the proposed apparatus shown in Fig. 1(b). The only difference was that the vertical-loading system was located above the specimen, including the load-cell measuring the vertical force also placed at the reaction side.

#### 2.1.2. V-shaped reaction force measurement link

When designing a force measurement link, the shear force and bending moment caused by the vertical displacement of the reaction beam must be maintained within the allowable range of the load cell included in the force measurement link. Therefore, the hinges at both ends of the force measurement links must have high axial stiffness, but low rotational stiffness. In this experiment, two types of force measurement links, one with a narrowed flat section (hereinafter referred to as “elastic pin”) and the other with a mechanical pin connection using a fork-end and pin (hereinafter referred to as “mechanical pin”), were implemented and compared.

##### (1) Elastic pin link

Fig. 4 shows pictures of the force measurement links with elastic pins. In the elastic pin link, a flat-section steel member (elastic pin) was attached to both ends of the load cell using screwed bolts and fixing nuts. In this case, the shear force and bending moment acting on the load cell caused by the vertical displacement of the reaction beam were within the allowable range of the load cell capacity because of the low bending stiffness of the elastic pin.

##### (2) Mechanical pin link

Fig. 5 shows pictures of force measurement links with mechanical pins. In the mechanical pin link, a machined steel fork-end is attached to both ends of the load cell. In this case, the bending moment at the joint is

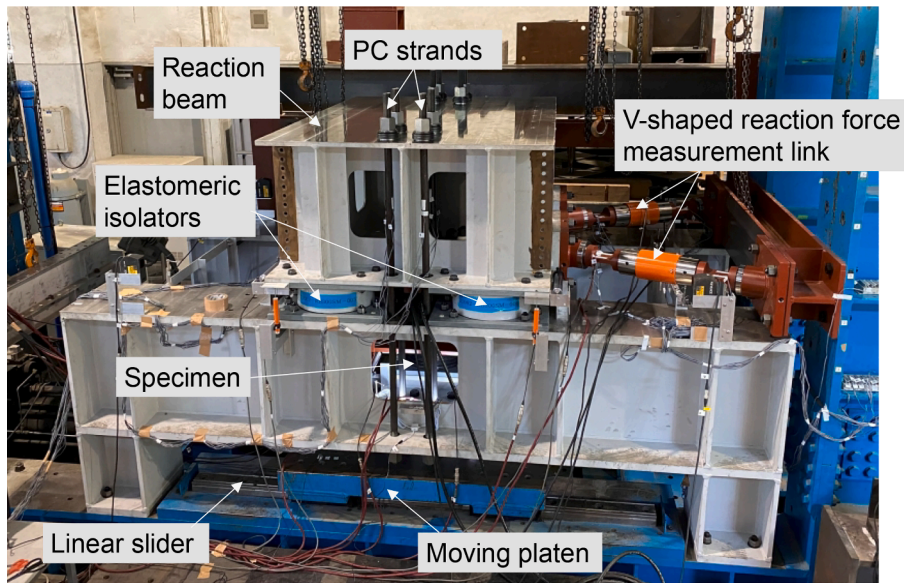


Fig. 2. Setup for mock-up experiment.

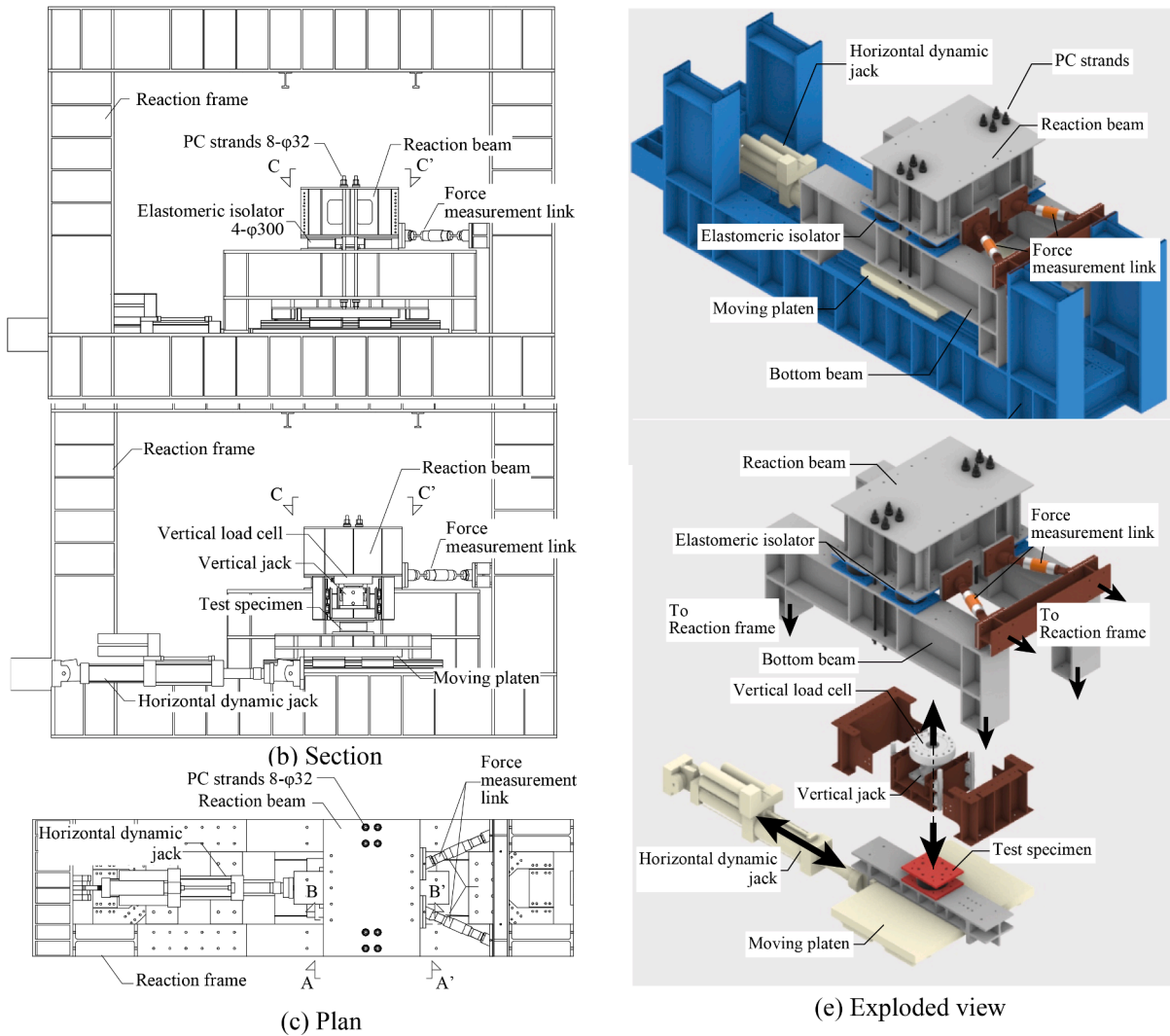


Fig. 3. Experimental setup and detail.

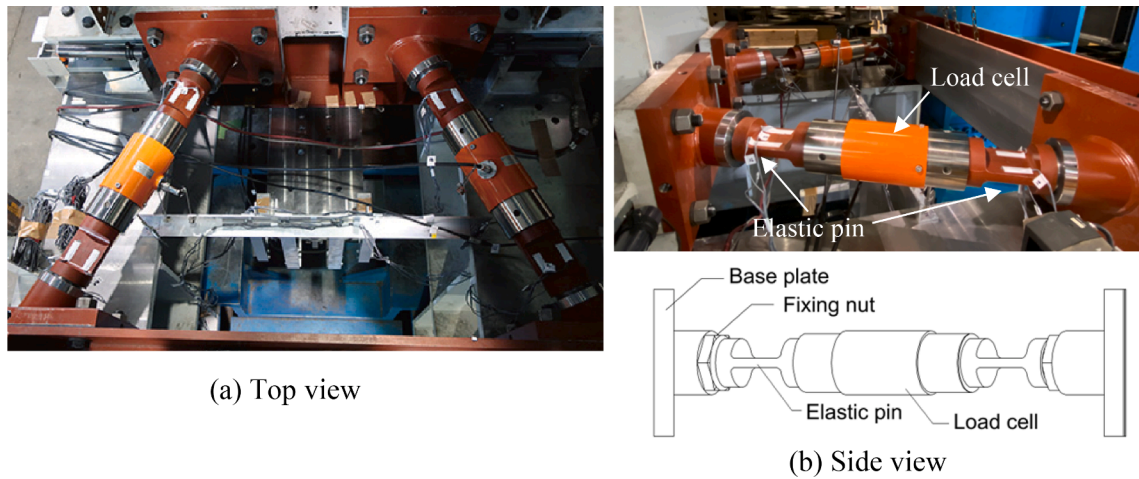


Fig. 4. Force measurement link with elastic pin.

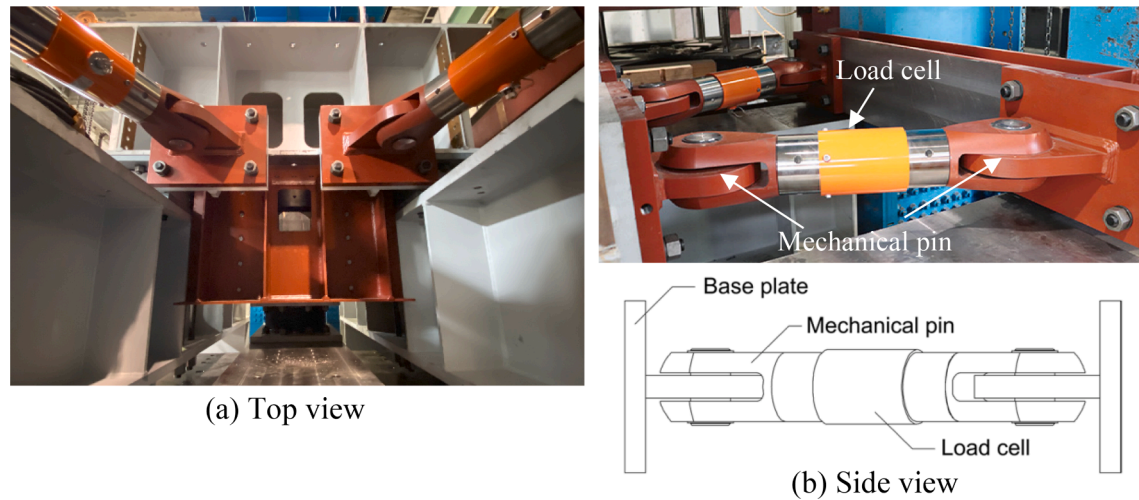


Fig. 5. Force measurement link photo with mechanical pin.

completely released, but there is a clearance of 0.2 ~ 0.3 mm at each pin joint, and rattling is expected to occur.

### 2.1.3. Elastomeric isolator supporting the reaction beam

For the elastomeric isolator supporting the reaction beam, first, the horizontal stiffness must be low to transfer most of the horizontal reaction force to the force measurement links with a load cell for accurate measurement; second, the vertical stiffness must be high to realize the vertical fixed boundary; and third, the horizontal reaction force of the elastomeric isolator must have a linear load-deformation relationship to accurately calculate the remaining reaction force regardless of the phase. Based on these requirements, laminated natural rubber bearings were used as elastomeric isolators to support the reaction beam, similar to the proposed full-scale facility. Separate small deformation experiments have confirmed that the laminated natural rubber bearing exhibits perfectly linear behavior within 1–2 mm deformation range, although the horizontal stiffness in this range is slightly higher than the horizontal stiffness value under 100% shear strain [9]. The horizontal reaction force was measured directly by adding the linear stiffness multiplied by the horizontal deformation of the bearing to the parallel components of the load-cell value of the force measurement links. If there is no rattling in the measuring links, the horizontal deformation of the laminated rubber bearing is simply equal to the amount of elastic deformation of the measuring links; therefore, the horizontal reaction

force sharing ratio of the laminated rubber bearing is expected to be less than 1–2% of the total horizontal reaction force.

Three types of 300 mm diameter laminated natural rubber bearing specimens from different manufacturers and shear modulus were used as the subjects of dynamic cyclic loading tests, and two types of force measurement links with load cells were used making a total of four setup configurations, as shown in Table 1.

## 2.2 Measurement plan

The typical measurement points are listed in Table 2 and Fig. 6. Each numerical value was calculated from the measured data, as discussed in this section.

### 2.2.1. Lateral displacement of the test specimen

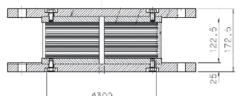
The horizontal displacement of the test specimen,  $\delta_h$ , was calculated by deducting the average horizontal deformation at four measurement points on the upper flange, from the average horizontal deformation measured at two points on the lower flange of the test specimen.

$$\delta_h = \frac{\delta_1 + \delta_2}{2} - \frac{\delta_3 + \delta_4 + \delta_5 + \delta_6}{4} \quad (1)$$

### 2.2.2. Horizontal reaction force of test specimen

The horizontal reaction force  $R$  of the specimen was calculated using

**Table 1**  
Tested specimen and link type.

Setup	Measurement link	Specimen	Rubber sheet thickness (mm)	Numbers of layer	Total rubber height (mm)	Total height (mm)	 Section of specimen B
RB-e-A <sub>1</sub>	Elastic pin	A <sub>1</sub> (G = 0.29)	2.25	26	58.5	116	
RB-e-A <sub>2</sub>	Elastic pin	A <sub>2</sub> (G = 0.39)	2.25	26	58.5	116	
RB-e-B	Elastic pin	B (G = 0.39)	2.25	26	58.5	98.5	
RB-p-B	Mechanical pin	B (G = 0.39)	2.25	26	58.5	98.5	

**Table 2**  
Measurement point list.

Variable	Measurement point	Measurement item	Unit
$P_A$	Horizontal dynamic jack	horizontal load	kN
$\Delta_A$	Moving platen	horizontal disp.	mm
$\delta_1$	Test specimen (lower plate)	horizontal disp.	mm
$\delta_2$	Test specimen (lower plate)	horizontal disp.	mm
$\delta_3$	Test specimen (upper plate)	horizontal disp.	mm
$\delta_4$	Test specimen (upper plate)	horizontal disp.	mm
$\delta_5$	Test specimen (upper plate)	horizontal disp.	mm
$\delta_6$	Test specimen (upper plate)	horizontal disp.	mm
$\delta_7$	Reaction beam	horizontal disp.	mm
$\delta_8$	Reaction beam	horizontal disp.	mm
$\delta_9$	Reaction beam	horizontal disp.	mm
$\delta_{10}$	Reaction beam	horizontal disp.	mm
$N_V$	Vertical load cell	vertical load	kN
$N_{L-A}$	Force measurement link	horizontal load	kN
$N_{L-B}$	Force measurement link	horizontal load	kN
$a_1$	Moving platen	acceleration	mm/s <sup>2</sup>

measurement links, horizontal force calculated from the deformation of the four elastomeric isolators supporting the reaction beam, and  $P\Delta$  force due to the initial tension of the PC-steel bar binding the reaction beam.

$$R_1 = -(N_{L-A} + N_{L-B}) \cdot \cos\theta + (4k' + k_{P\Delta}) \cdot \left( \frac{\delta_7 + \delta_8 + \delta_9 + \delta_{10}}{4} \right) \quad (2)$$

where the angle between the V-shaped links and the loading direction  $\theta = 23.9^\circ$ , the horizontal stiffness  $k' = 0.58$  kN/mm ( $G = 0.39$ , B-type) for the bearing under small deformation, and the  $P\Delta$  stiffness  $k_{P\Delta} = 1.14$  kN/mm as a result of the pretention in the PC-steel bars.

### (2) Conventional measurement system

The horizontal reaction force,  $R_2$ , in the conventional reaction force measurement system was obtained using a load cell in a horizontal dynamic jack. This value includes the effects of friction and inertial forces.

$$R_2 = P_A \quad (3)$$

### (3) Linear model

As a reference, the horizontal reaction force  $R_3$  was calculated from the horizontal stiffness  $k$  of the laminated rubber specimen in the manufacturer catalog and the shear deformation.

$$R_3 = k \cdot \delta_h \quad (4)$$

where the horizontal stiffness of the laminated rubber specimens is  $k = 0.47$  kN/mm (shear modulus  $G = 0.39$  N/mm<sup>2</sup>) and  $k = 0.35$  kN/mm (shear modulus  $G = 0.29$  N/mm<sup>2</sup>) for 100% shear strain (approximately 58.5 mm).

### 2.3 Loading matrix

Table 3 shows the loading matrix. Sine waves of varying amplitude, frequency, vertical pressure, and number of cycles were applied to the laminated rubber bearing specimens. The tests are carried out with all possible combinations of the parameters given in this table.

## 3. Experimental results

### 3.1 Reaction force

#### (1) Elastic pin link

This section describes the results of loading specimen B ( $G = 0.39$ )

**Table 3**  
Loading conditions.

Parameter		Range of variable
Frequency	$f$ (Hz)	0.05 (quasi-static), 0.2, 0.5, 1.0, 2.0
Amplitude	$A$ (mm)	2, 5, 10, 20, 30, 50, 100, 150
Compression	$\sigma$ (MPa)	0, 5, 10, 15
Number of cycle	-	2 (quasi-static), 10, 15 (2 Hz)

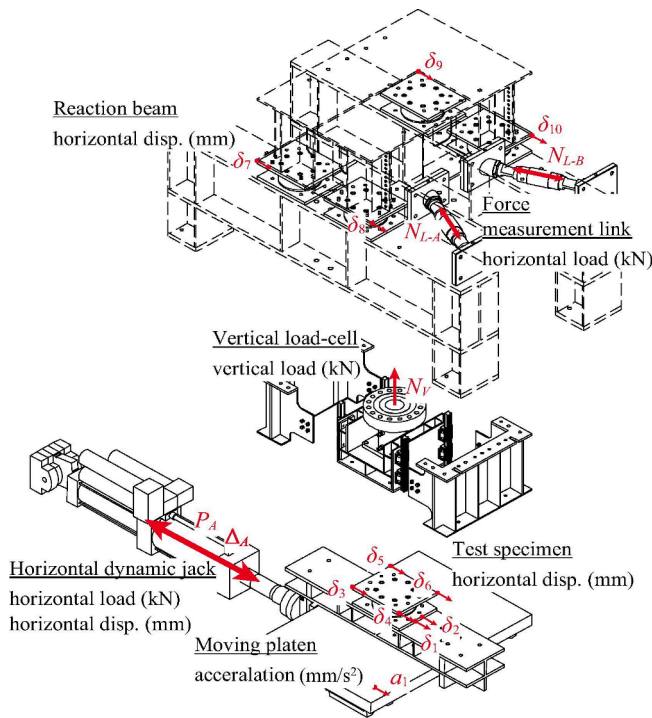


Fig. 6. Measurement points.

the following three methods.

#### (1) Proposed measurement system

The horizontal reaction force  $R_1$  in the proposed reaction force measurement system was obtained as the sum of the horizontal component of the forces acting on the load cell with V-shaped force

and discusses the effects of the proposed reaction force measurement system with elastic pin links.

Fig. 7 shows the relationship between the horizontal deformation and horizontal reaction force for the tests with quasi-static ( $f = 0.05$  Hz) loading, compression  $\sigma = 0$  MPa, and amplitudes  $A = \pm 2, 20,$  and  $100$  mm. Because the loading velocity was low and no vertical pressure was applied, inertial and frictional forces that could cause measurement errors were not generated, and the results indicated that  $R_1$  and  $R_2$  were close. In addition, in the medium-amplitude range, the linear stiffness indicated by the green line is generally in agreement with the stiffness at 100% shear strain (corresponding to 58.5 mm shear deformation). The measured stiffness was slightly higher for lower amplitudes of  $A = 2$  mm and lower in higher amplitudes of  $A = 100$  mm.

Fig. 8 shows the horizontal displacement-horizontal reaction force relationship at amplitudes of  $A = \pm 2, 20,$  and  $100$  mm at a frequency  $f = 1.0$  Hz, where the loading velocity is increased while maintaining the compression  $\sigma = 0$  MPa. It can be observed from these graphs that errors were generated between  $R_1$  and  $R_2$ . These errors increased with acceleration as the sinusoidal amplitude increased, which can be explained by the inertial force being proportional to the acceleration.

Fig. 9 shows the horizontal deformation-horizontal reaction force relationship for amplitudes  $A = \pm 2, 20,$  and  $100$  mm at a compression of  $\sigma = 15$  MPa under quasi-static loading. It can be seen from these plots that there is a large error between  $R_1$  and  $R_2$ , especially in the small amplitudes due to the frictional force between the moving platen and linear sliders, which is proportional to the compression. The frictional force was maintained between 6 and 9 kN. Because the vertical load was 100 kN, the linear slider had a friction coefficient equivalent to  $\mu = 0.06$ – $0.09$ . In Fig. 9(b), a reaction spike was observed near the zero displacement in  $R_2$  graph. This was attributed to the slight denting in the linear slider surface of this particular test setup caused by numerous preliminary compression tests. Finally, Fig. 10 shows the horizontal reaction force-horizontal deformation-relationship for  $f = 1$  Hz,  $\sigma = 15$  MPa, and amplitudes  $A = \pm 2, 20,$  and  $100$  mm, with dynamic loading and vertical load. In these graphs, the influence of the inertial force shown in Fig. 8 and that of the friction force shown in Fig. 9 coexist. From Figs. 8–10, the measured values of the proposed measurement links are stable and unaffected by friction and inertial forces, even in a small deformation range.

## (2) Mechanical pin link

Fig. 11 shows the relationship between the horizontal displacement and horizontal reaction force when mechanical pins were used as measurement links for the tests with  $A = \pm 100$  mm, (a) quasi-static loading, axial pressures of  $\sigma = 0$ , (b)  $f = 1$  Hz,  $\sigma = 0$  MPa, and (c)

quasi-static loading,  $\sigma = 15$  MPa compression. In Fig. 11 (a) and (c), where quasi-static loading was applied, the horizontal reaction force was accurately measured using the proposed link, similar to the elastic pin link. In contrast, in Fig. 11 (b), a large noise is observed near the zero displacement with a large loading velocity. This is owing to the impact force generated when the pin gap collides, which will be discussed later in this paper.

## 3.2. Friction and inertia force

As discussed in Section 3.1, the measured reaction force  $R_1$  by the proposed reaction force measurement system using the elastic pin link is considered to accurately measure the horizontal reaction force, excluding the inertial force  $F_{iner}$  (kN) and friction force  $F_{fric}$  (kN) applied to the moving platen. The influence of these errors on the measured reaction force  $R_2$  (kN) due to inertia and friction force was analyzed based on the results of loading using the results of the elastic pin link with specimen B. The frictional and inertial forces were evaluated using the following equations:

$$F_{error} = R_1 - R_2 \quad (5)$$

$$F_{iner} = m \cdot a_1 \quad (6)$$

$$F_{fric} = F_{error} - F_{iner} \quad (7)$$

where  $m$  is the mass of the moving platen (1,200 kg), and  $a_1$  ( $m/s^2$ ) is the acceleration of the table.

Fig. 12 shows the relationship between the horizontal deformation of the specimen and various errors for  $f = 1$  Hz,  $\sigma = 0$  MPa, and  $A = \pm 2, 20,$  and  $100$  mm. Because the magnitude of inertial force is proportional to the acceleration and the maximum value of the horizontal reaction force of the specimen, the percentage of error is almost constant for the same frequency of loading, which is approximately 30–40% for dynamic loading at  $f = 1$  Hz. As shown in the same figure, the inertial force  $F_{iner}$  (kN) calculated from the acceleration of the moving platen and the total measurement error  $F_{error}$  (kN) were almost identical in the range where there was no compression. This indicates that the error due to the inertial force can be evaluated for regular excitations such as sinusoidal waves by applying theoretical Equation (6).

Fig. 13 shows the relationship between the horizontal deformation and the error for quasi-static loading,  $\sigma = 15$  MPa compression, and  $A = \pm 2, 20,$  and  $100$  mm. Because of the quasi-static load, the error is considered to be due only to the frictional force. The frictional force is proportional to the vertical pressure and is generally constant regardless of the amplitude, except for the effect of the imperfections in the linear slider. The smaller the amplitude and the horizontal reaction force of the

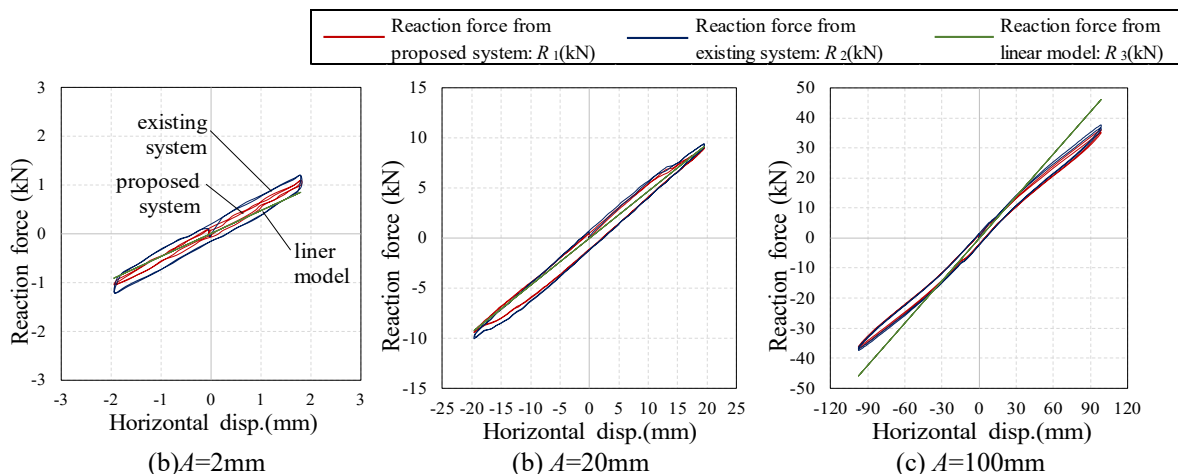


Fig. 7. Reaction force- deformation relationship: quasi-static ( $f = 0.05$  Hz) loading, no-compression.

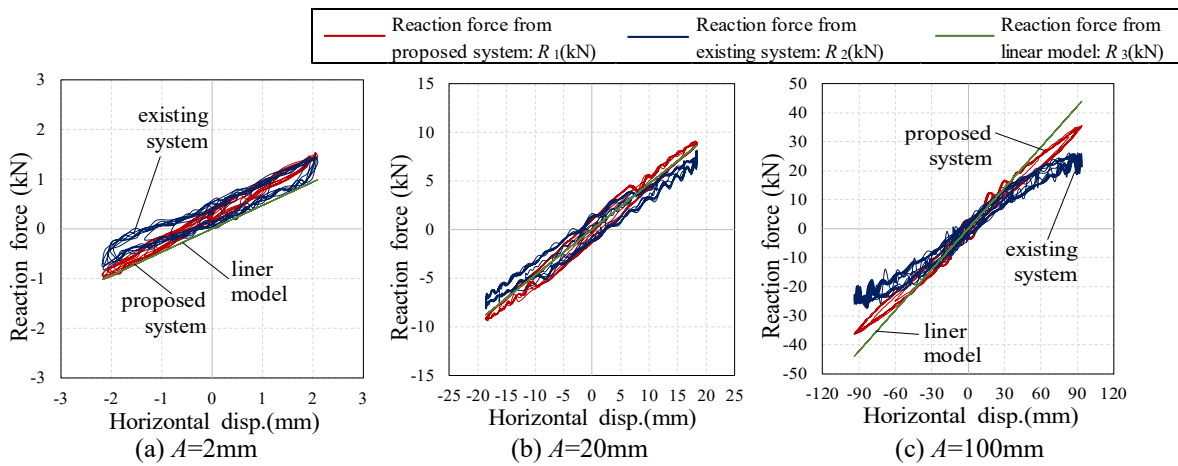


Fig. 8. Reaction force-deformation relationship: dynamic loading ( $f = 1.0$  Hz), no-compression.

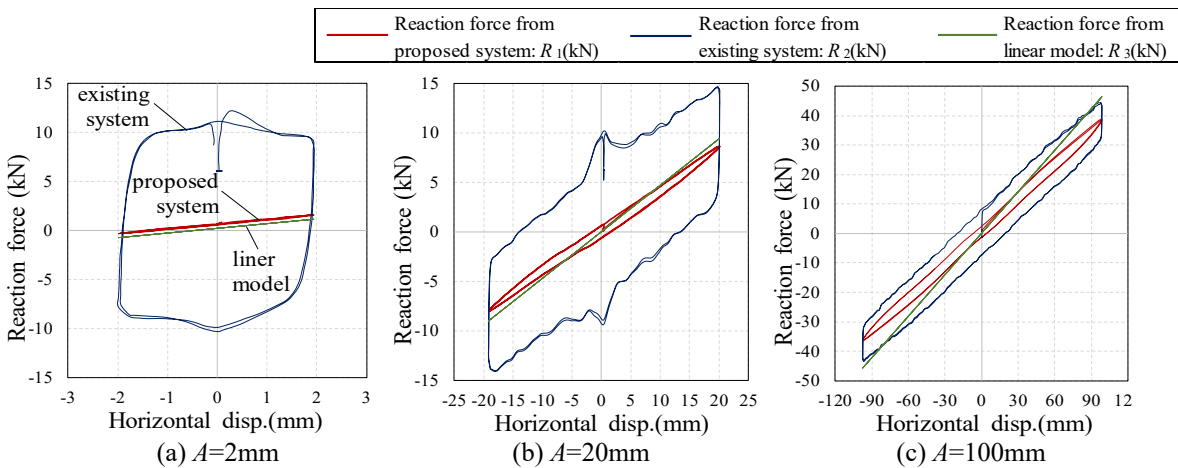


Fig. 9. Reaction force-deformation relationship: quasi-static ( $f = 0.05$  Hz) loading, with 15 MPa compression.

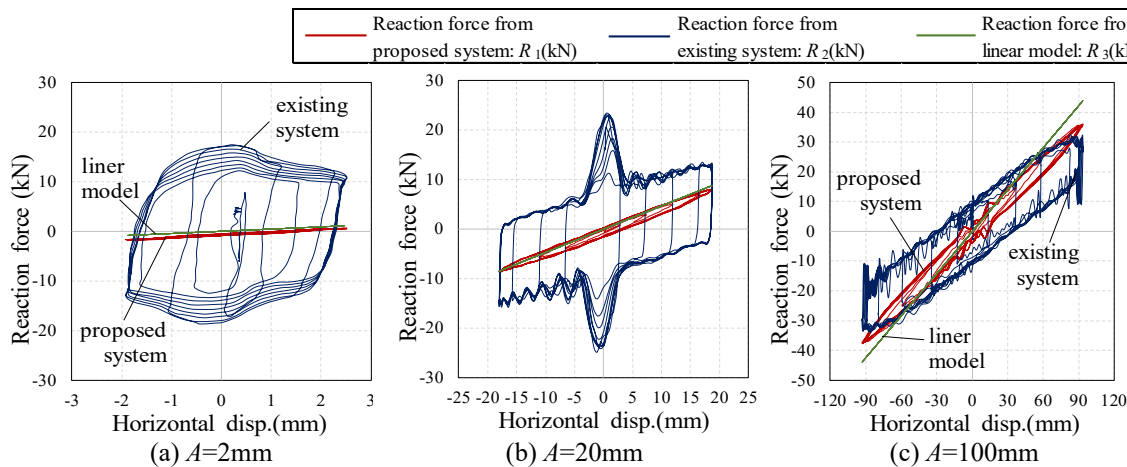


Fig. 10. Reaction force-deformation relationship: dynamic loading ( $f = 1.0$  Hz), with 15 MPa compression.

specimen, the larger is the error percentage. In Fig. 13 (a), the test results for amplitude  $A = \pm 2$  mm, the error is about 12 times the maximum horizontal reaction force. In Fig. 13 (c), the test results for amplitude  $A = 100$  mm, the error reaches approximately 20% of the maximum horizontal reaction force. Furthermore, the variation in friction forces due to the effect of the denting in the linear slider, as shown in Fig. 13 (b)

$A = \pm 20$  mm test results, is dependent on the condition of the individual test machine, making it difficult to model and filter the friction force in a practical manner.

Fig. 14 shows the relationship between the horizontal displacement and various errors in the test results for  $f = 1$  Hz,  $\sigma = 15$  MPa, and  $A = \pm 2, 20,$  and  $100$  mm. Although the inertial force is not affected by the



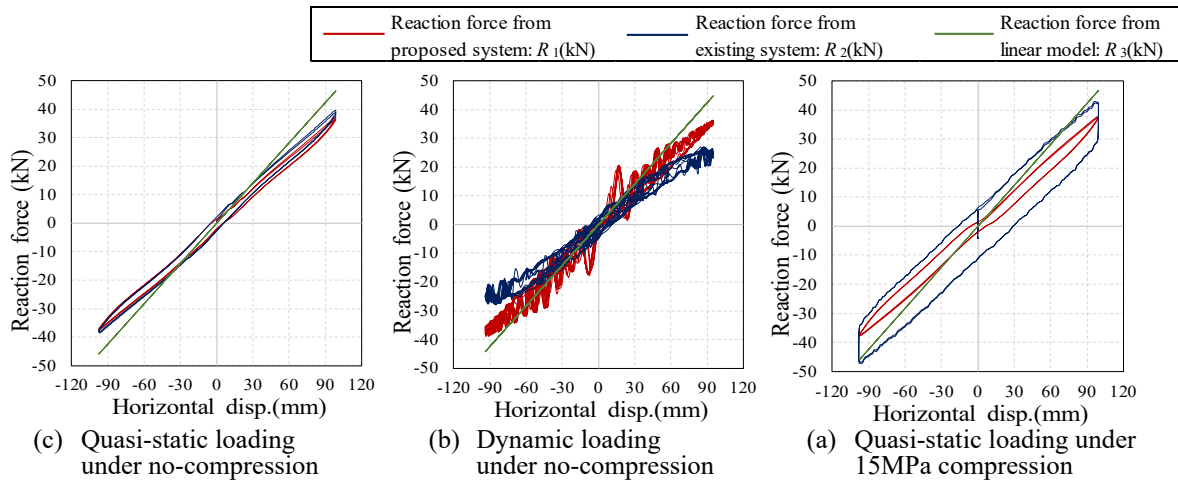


Fig. 11. Reaction force-deformation relationship with mechanical pin link.

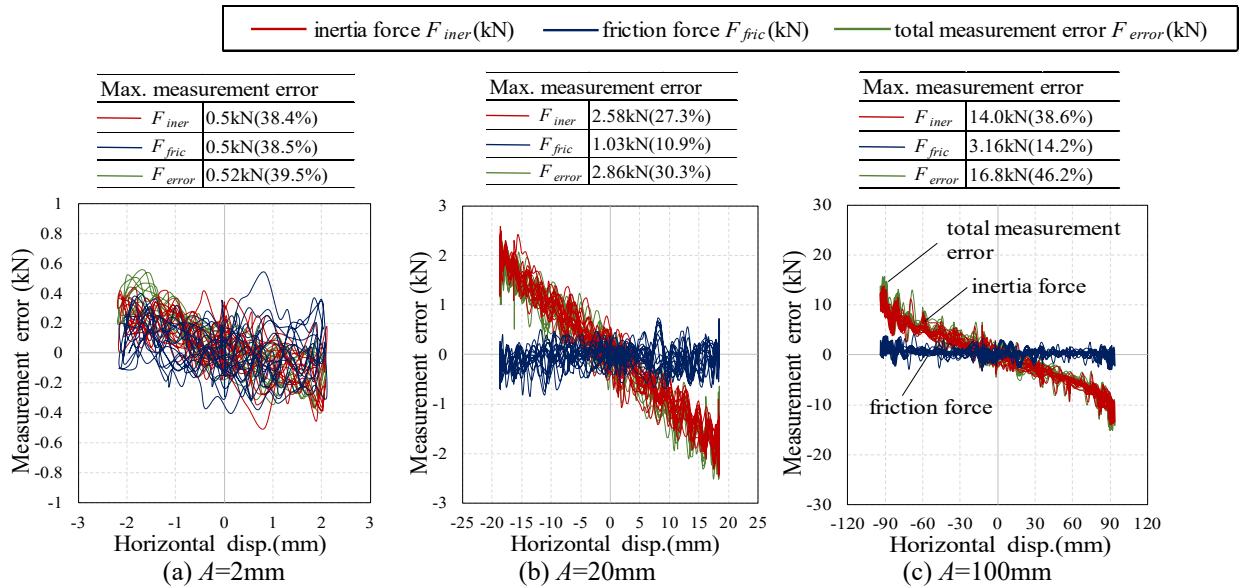


Fig. 12. Measurement error in dynamic loading ( $f = 1.0\text{ Hz}$ ), no-compression.

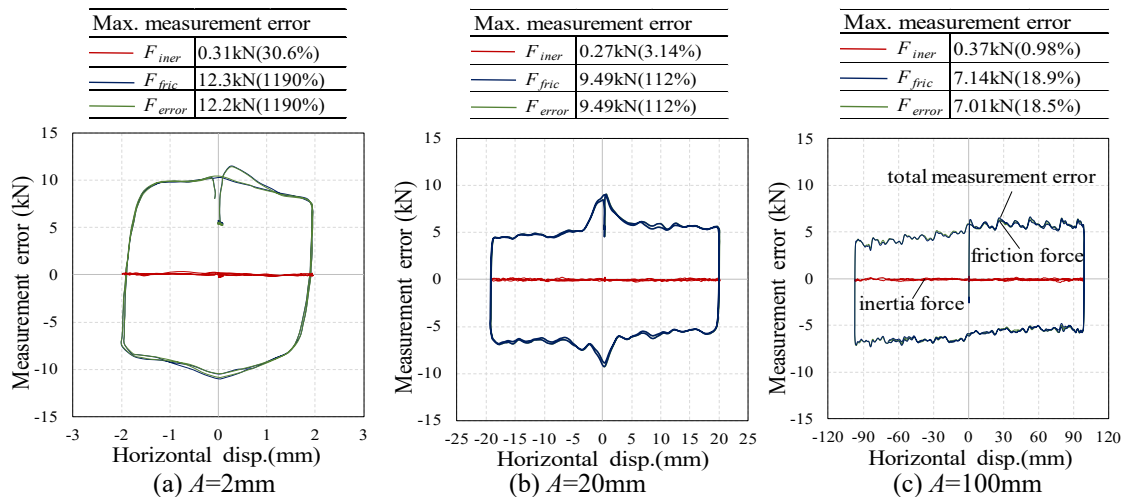


Fig. 13. Measurement error in quasi-static ( $f = 0.05\text{ Hz}$ ) loading under 15 MPa compression.

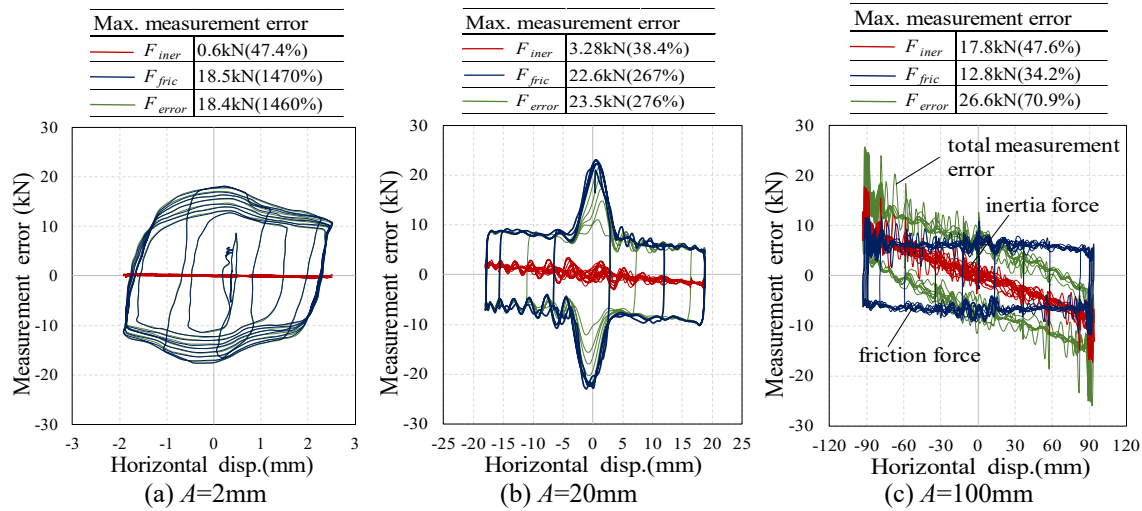


Fig. 14. Measurement error in dynamic loading under 15 MPa compression.

surface pressure and the error rate is almost constant, the friction force changes in each loop under dynamic loading. This indicates that the frictional force is difficult to precisely model and filter.

### 3.3. Force contribution ratio

The contribution ratio of the horizontal reaction force between the force measurement links and elastomeric isolator supporting the reaction beam in  $R_1$  was investigated. Each reaction force component and their ratios were evaluated using the following equations:

$$R_{link} = \frac{-(N_{L-A} + N_{L-B}) \cdot \cos\theta}{R_1} \quad (8)$$

$$r_{link}(\%) = \frac{R_{link}}{R_1} \times 100 \quad (9)$$

$$R_{rb} = \frac{(4k' + k_{P\Delta}) \cdot (\delta_7 + \delta_8 + \delta_9 + \delta_{10})}{R_1} \quad (10)$$

$$r_{rb}(\%) = \frac{R_{rb}}{R_1} \times 100 \quad (11)$$

where  $R_{link}$  (kN) denotes the force measurement link horizontal reaction force;  $r_{link}$  (%) denotes measurement link reaction force ratio;  $R_{rb}$  (kN) denotes the elastomeric isolator bearing horizontal reaction force; and  $r_{rb}$  (%) denotes the elastomeric isolator bearing horizontal reaction force.

Figs. 15 and 16 show the time-history transitions of the reaction

forces  $R_{link}$  (kN) and  $R_{rb}$  (kN) from the test results for  $f = 1$  Hz,  $\sigma = 15$  MPa,  $A = \pm 2$ , and 100 mm.

#### (1) Elastic pin link

Fig. 15 shows that, 95 ~ 97.5% of the measured reaction force  $R_1$  from the proposed reaction force measurement system acts on the measurement link and 2.5 ~ 5% acts on the elastomeric isolators. Although this value is slightly larger than the expected value evaluating the elastic axial deformation of the measurement link, it can be confirmed that the majority of the measured reaction force acts on the force measurement link. This difference is attributed to the rattling in the threads of the connecting bolts used for the measurement link.

#### (2) Mechanical pin link

Fig. 16 shows that when mechanical pins are used, approximately 70 ~ 95% of the measured reaction force acts on the force measurement links and 5 ~ 30% on the elastomeric isolators, with a large variation that is particularly noticeable at small amplitudes. This is attributed to rattling caused by clearance around the mechanical pin, which is difficult to omit. This rattling is also thought to have caused the noise observed in the Section 3.1 (2).

### 3.4 Evaluation of each measurement link

Based on the aforementioned results and discussion, it can be concluded that the horizontal force measurement link with the elastic

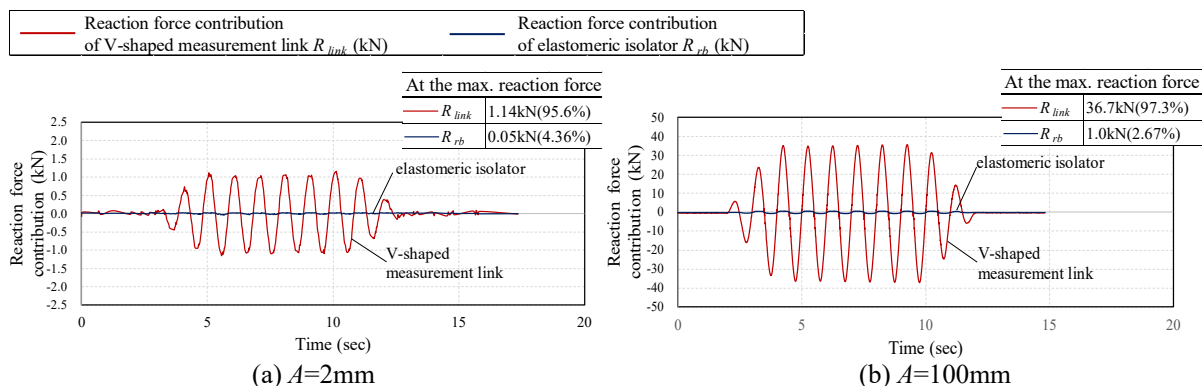


Fig. 15. Reaction force contribution with Elastic pin link.

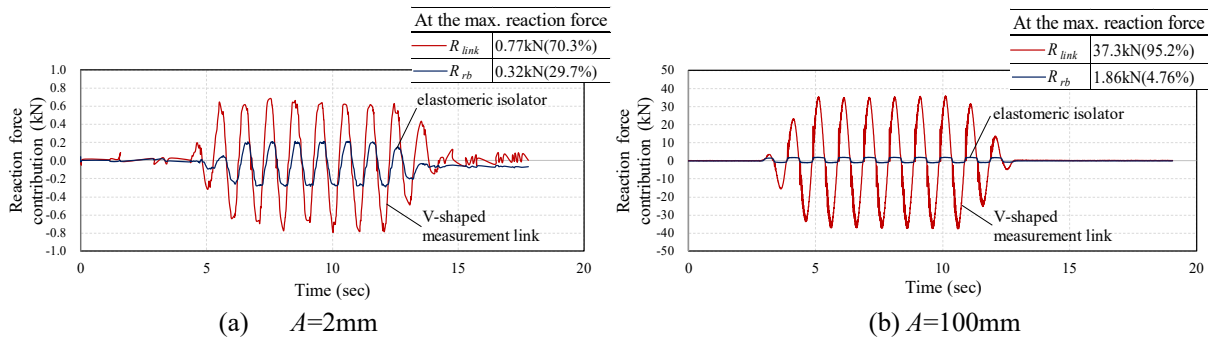


Fig. 16. Reaction force contribution with Mechanical pin link.

pin is superior to the mechanical pin link in terms of the magnitude of the noise appearing in the measurement reaction force and the high and stable force contribution ratio against the elastomeric isolators. However, even with the elastic pin link, there were cases where small noise was generated in the measurement reaction force, or the distribution ratio to the elastomeric isolator was relatively high, especially under small amplitudes. This could be due to the rattling of the measurement link joint screws or loosening of the tightening nut. For application to full-scale testing facilities, it is desirable to install fixing nuts on all the connecting screws that prevents any looseness at the threads. The noise that slightly appeared in the dynamic measurement force could be sufficiently corrected by lowering the cutoff frequency of the low-pass filter, and it was confirmed that the total reaction force, which is the sum of the reaction force of the measurement link and elastomeric isolator, was stable and accurate even when the contributing ratio of the

elastomeric isolator became larger.

#### 4. Accuracy verification test for the proposed measurement system

In this setup, the laminated rubber test specimen and vertical loading system is replaced with a load-cell unit (hereinafter referred to as “load-cell specimen”), and quasi-static loading test is conducted to confirm the accuracy of the proposed force measurement system.

##### 4.1 Experimental setup

A diagram of the test setup is shown in Fig. 17 (a) and (b), and the basic setup components are shown in Fig. 17 (c). A picture of the load-cell specimen is shown in Fig. 17 (d). The test apparatus consists of, from

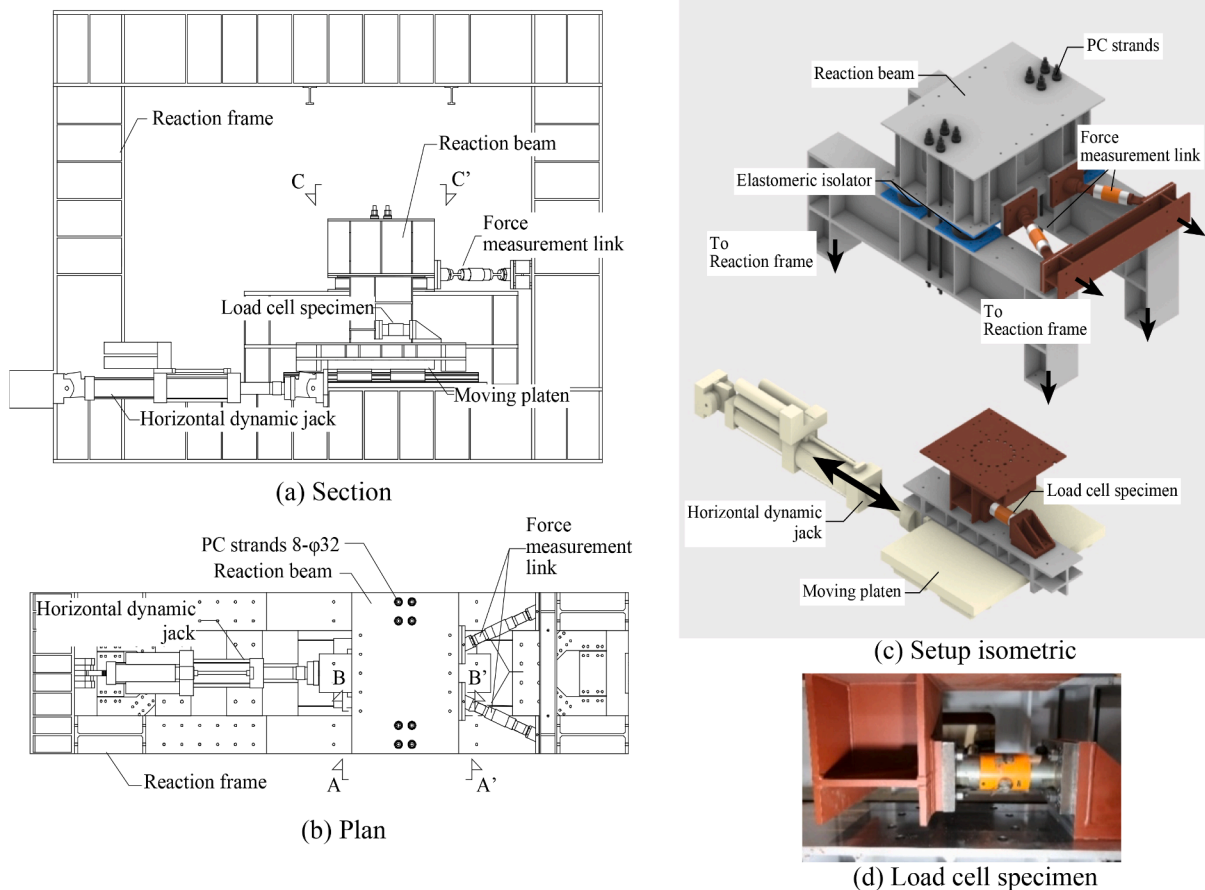


Fig. 17. Setup details for accuracy verification test.

the bottom, a moving platen, a load-cell specimen, and a reaction beam. The force measurement links the load cells attached to the side of the reaction beam, similar to the configuration of the dynamic mockup tests described in Section 2. Elastic pin links were used as measurement links. In this configuration, the moving platen was loaded positively and negatively with quasi-static incremental loading, without vertical loading.

## 4.2 Experimental results

### 4.2.1. Comparison with load-cell specimen

Fig. 18 shows a plot of  $N$  (kN) from the load-cell specimen on the horizontal axis, and the link value  $R_1$  (kN) and dynamic jack load-cell value  $R_2$  (kN) on the vertical axis. The closer the plots were to the 45° line, the more they correspond to each other. The measurement results obtained with maximum loadings of  $\pm 200$  kN and  $\pm 500$  kN are shown. In the graphs, plots almost perfectly aligns with the 45° line, where, less than 1% error have been observed for  $R_1$  and the error was approximately 2% for  $R_2$ .

Fig. 19 plots  $R_1$  (kN) on the horizontal axis and  $r_{link}$  and  $r_{rb}$  (%) on the vertical axis as a percentage of  $R_1$  for  $R_{link}$  and  $R_{rb}$  (kN). The figures show that the distribution ratio of  $r_{link}$  reaches a peak ( $r_{link} = 94.3\%$ ,  $r_{rb} = 5.7\%$ ) at about  $R_1 = 20$  kN and then converges to  $r_{link} = 99.2\%$  and  $r_{rb} = 0.8\%$ . This peak is considered to be the region where rattling of the measurement link joint screws occurs, as mentioned earlier.

## 5. Dynamic characteristics of natural rubber bearing under small amplitude

To date, the accurate dynamic response characteristics of laminated rubber bearings under small amplitude of 1–2 mm have not been clarified accurately because existing reaction force measurement systems in test machines include large errors caused by friction and inertia. However, with the proposed force measurement system, these micro-deformation characteristics now can be accurately measured without frictional and inertial forces. For using the laminated rubber bearings for the elastomeric isolators for the proposed force measurement system, confirming the linearity and exact stiffness of these laminated rubber bearings under 1–2 mm amplitude is essential. Also, evaluating the response of seismically isolated structures under wind forces, exact stiffness measurements with smaller amplitudes are required. Such stiffness under smaller amplitudes has never been obtained using the existing test machines because of the contamination of friction. This section reports the dynamic response characteristics of three types of natural rubber bearings used as test specimens, particularly the dependence of the horizontal stiffness with equivalent damping on the vertical

pressure and vibration frequency during micro-deformation ( $A = \pm 2$  mm).

Figs. 20 and 21 show the horizontal stiffness  $k$  (kN/mm) and equivalent damping ratio  $h_{eq}$  (%) on the vertical axis, vertical pressure  $\sigma$  (MPa) on the horizontal axis, and frequency  $f$  (Hz) as a parameter for each test result for a small amplitude of  $A = \pm 2$  mm. The horizontal stiffness values in each plot were calculated using the least-squares method based on the data obtained by setting the cutoff frequency  $f_c$  (Hz) of the low-pass filter to 20 Hz for the measured reaction force in the loading protocol. The equivalent damping ratio was calculated from the total dissipated energy divided by the averaged elastic strain energy, and  $4\pi$ .

From Fig. 20, it was confirmed that the horizontal stiffness of each natural rubber bearing specimen varied approximately  $\pm 15$ –20% from the median of the maximum and minimum values under micro deformation when mainly the vertical pressure was varied. In addition to the horizontal stiffness decreasing with increasing vertical pressure, there was also a slight vibration frequency dependence, in which the horizontal stiffness increased with increasing frequency, although each load–displacement relationship was completely linear. Equivalent damping ratio in Fig. 21 varies between 2 and 6% for the specimens A1 and A2, and varies between 4 and 8% for the specimen B. Although no clear dependency on vertical pressure and frequency was observed, damping in dynamic loadings tend to be higher than quasi-static loadings ( $f = 0.05$  Hz). Fig. 22 shows the amplitude dependence of the stiffness. Both in  $G = 0.29$  and  $G = 0.39$  laminated rubber bearings, the stiffness in smaller amplitudes less than 10 mm tended to be higher than over 100% (58.5 mm) amplitude.

## 6. Hybrid simulation using proposed measurement system

Hybrid simulation experiments using the measured horizontal reaction force from the proposed reaction force measurement system and the measured dynamic jack load-cell reaction force, including the friction force on the horizontal linear slider of the moving platen and inertial force, were conducted to compare the results and discuss the effectiveness of the proposed measurement system.

### 6.1 Building model

An actual two-story seismically isolated building, as shown in Fig. 23, was assumed as the model building for the hybrid simulation [10]. The analytical model is a shear-spring model with three masses and stiffness, as shown in Fig. 24. The horizontal stiffness of the isolation layer was 16 kN/mm with a damping ratio of 20%, including the additional damping by the isolation layer. Damping for the super-

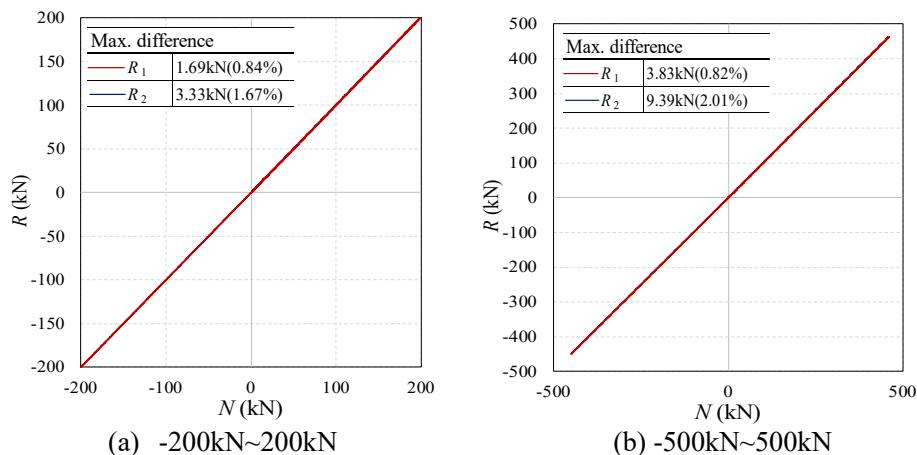


Fig. 18. Measured reaction force vs load-cell specimen value.

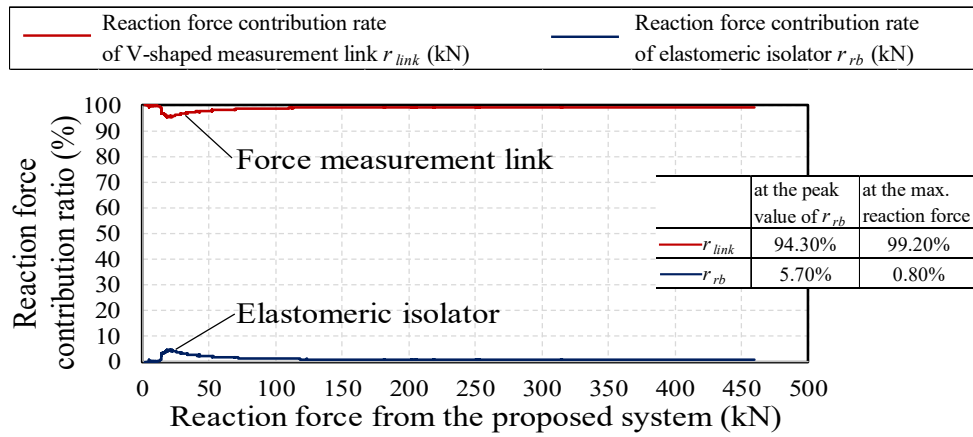


Fig. 19. Reaction force contribution.

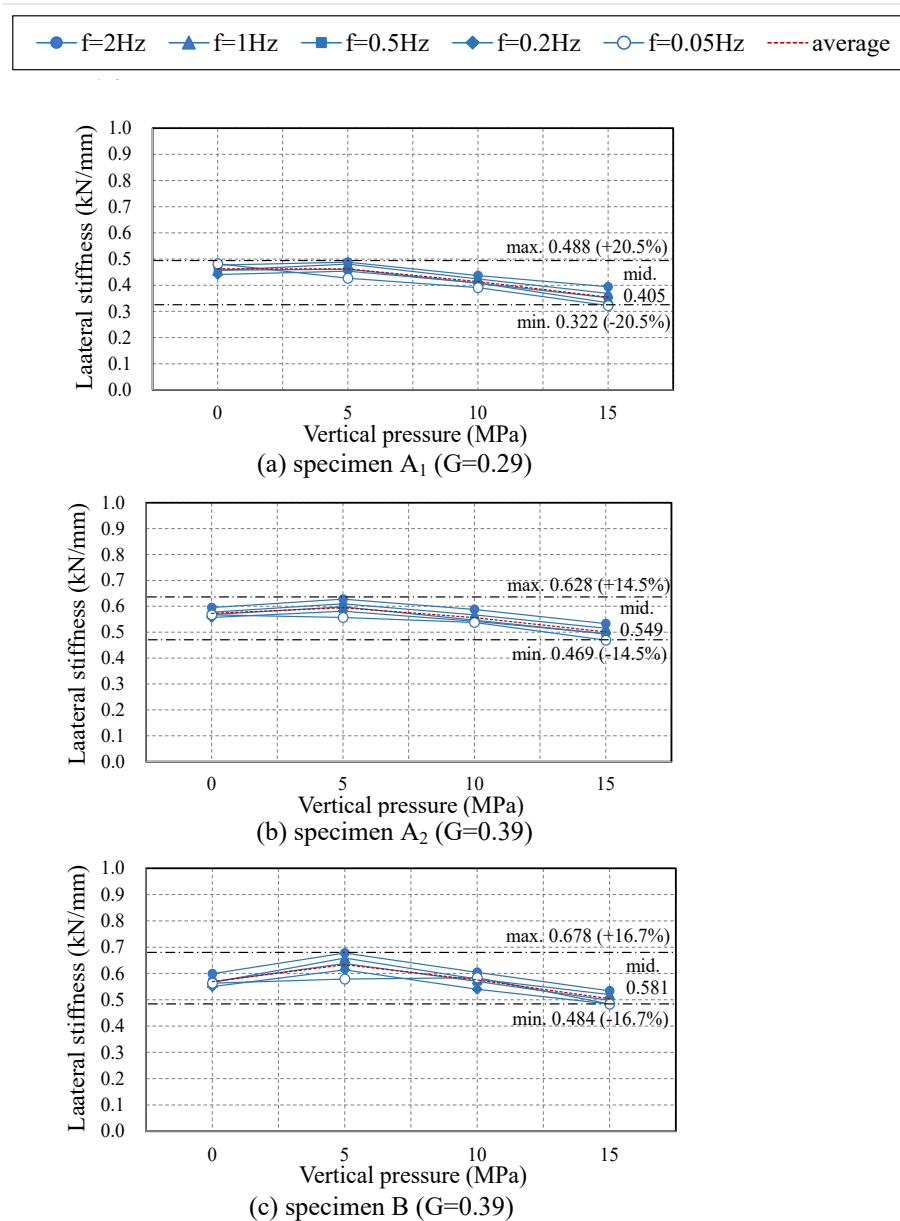


Fig. 20. Effects of pressure and frequency on lateral stiffness ( $A = \pm 2$  mm).

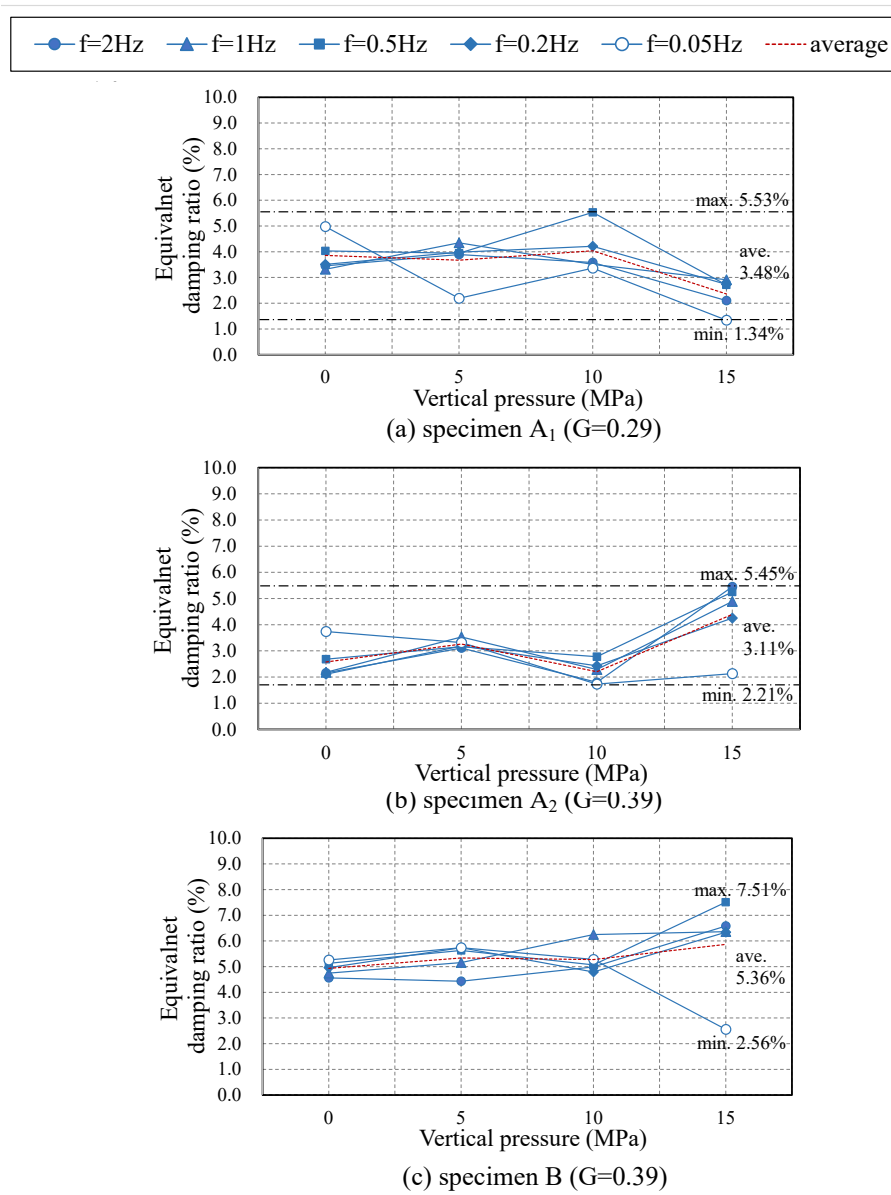


Fig. 21. Effects of pressure and frequency on damping ratio ( $A = \pm 2$  mm).

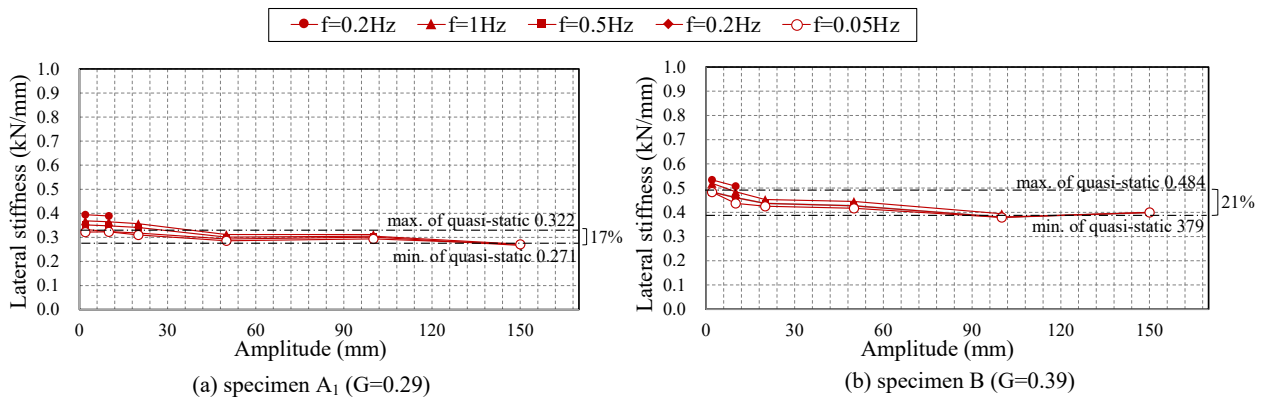


Fig. 22. Effects of amplitude on lateral stiffness (15 MPa compression).



Fig. 23. Building image.

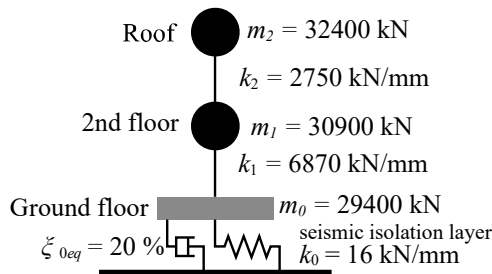


Fig. 24. Dynamic model.

**Table 4**  
Scale factors for hybrid simulation.

Parameter	Conversion multiplier (Experiment to Analysis)
Horizontal disp. (mm)	$\times 2.33$
Horizontal stiffness (kN/mm)	$\times 40$
Horizontal force (kN)	$\times 93.2$

structures was set to 2%. The scale factors between the virtual building model and the actual seismic isolation bearing specimen in the hybrid simulation was set, as shown in Table 4.

### 6.2 Input seismic motion

The input seismic motion was the Hachinohe EW wave, which have been matched to the design spectrum for a Level 2 earthquake defined in

Equations (12) ~ (13). Hybrid simulations were performed for Level 2 seismic motion which corresponds to an event with 475 years return period according to the Japanese code and a Level 1 seismic motion which is 1/5 of a Level 2 motion and corresponds to an event with 43 years return period. The seismic response spectra for Level 2 motion are shown in Fig. 25. In the spectra, the solid line shows the seismic spectrum after calibration and the dashed line shows the calibrated target spectrum.

$$S_A = \begin{cases} 3200 + 30000T & (T \leq 0.16) \\ 8000 & (0.16 < T < 0.64) \\ 5120/T & (0.64 \leq T) \end{cases} \quad (12)$$

$$S_V = S_A T / 2\pi \quad (13)$$

where the damping ratio  $\xi = 5\%$ , building natural period  $T$  (s), acceleration response spectrum  $S_A$  ( $\text{mm/s}^2$ ), and velocity response spectrum  $S_V$  ( $\text{mm/s}$ ).

### 6.3 Hybrid simulation setup

Fig. 26 shows a schematic diagram of the hybrid simulation setup, which uses the measured reaction force from the proposed reaction force measurement system with the force measurement links in Fig. 26 (a) and the dynamic jack load-cell force including frictional and inertial forces in Fig. 26 (b). OpenSees was used for the numerical analysis, and OpenFresco was used to connect the numerical model to the actual test system [11,12]. In the hybrid simulation, Explicit Newmark's  $\beta$  algorithm based on the average acceleration method ( $\beta = 0.25, \gamma = 0.5$ ) was used to calculate the displacement, velocity, and acceleration of each mass point at step  $n$  in the numerical analysis model.

### 6.4 Hybrid simulation results

Natural rubber bearing B is used for the specimen, and the virtual building response is evaluated by examining the difference between the hybrid simulation results using the force measurement link (proposed system), the results using the dynamic jack load cell (existing system), and the numerical analysis value as the reaction force which estimates the bearing stiffness as constant (linear system). The obtained horizontal displacement time-history curve and the relationship between the displacement and reaction force at the isolation layer from the hybrid simulation under Level 2 and Level 1 motions are shown in Figs. 27 and 28, respectively.

#### 6.4.1. Level 2 earthquake motion

Fig. 27 shows the results of the hybrid simulation for the Level 2 earthquake motion. As shown in Fig. 27 (a), the top displacement based on the proposed reaction force measurement system approximately the same as the linear system with numerical analysis value. The hysteresis of the proposed system in Fig. 27 (b) reflects the accurate nonlinear

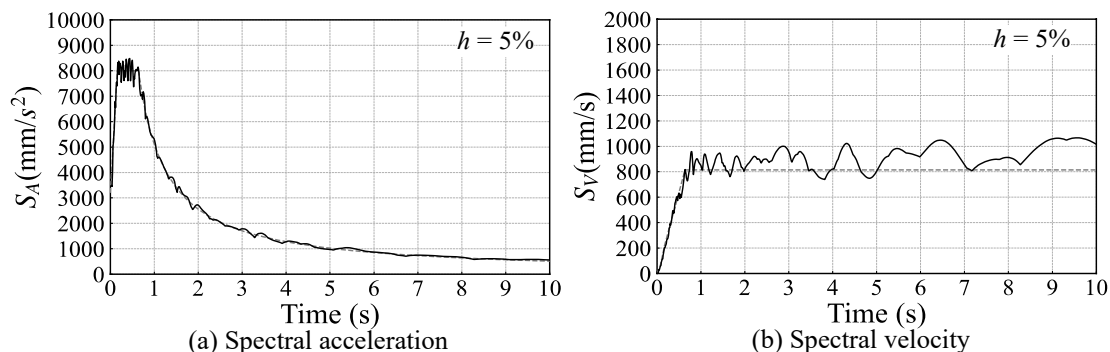


Fig. 25. Input seismic wave spectra.

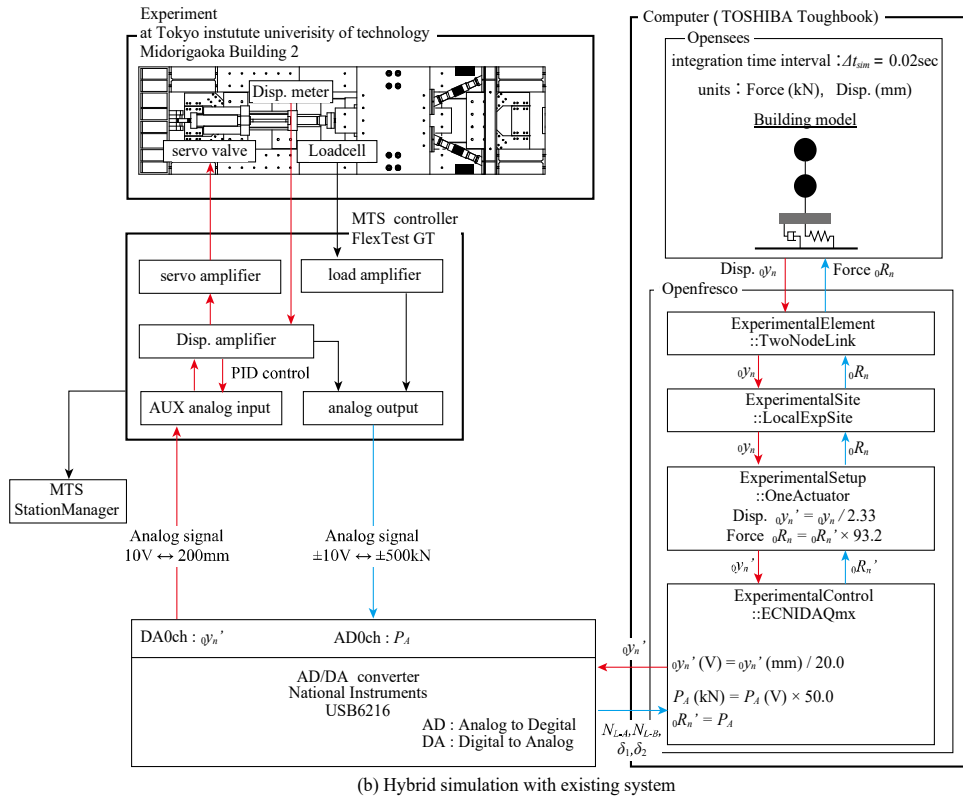
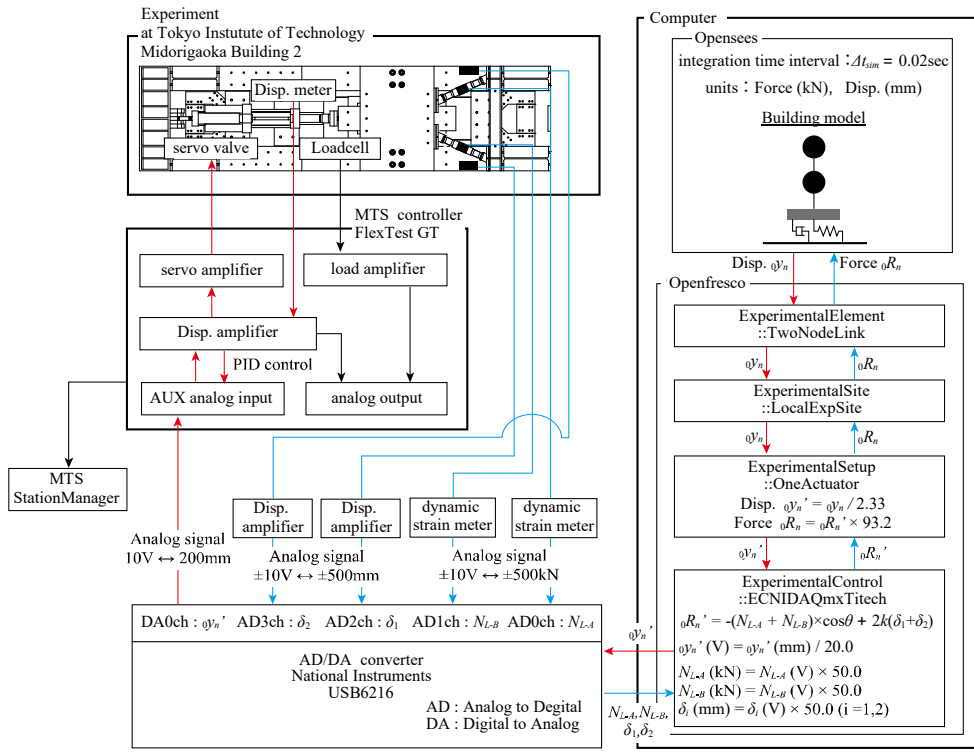


Fig. 26. Schematic diagram for hybrid simulation.

hysteresis of the rubber bearing, which indicates a more realistic response. The maximum value of the top displacement of the existing system based on the conventional reaction force measurement system is significantly smaller ( $-30\%$ ) than that of the proposed system.

#### 6.4.2. Level 1 earthquake motion

Fig. 28(a) shows that the simulation result using the proposed measurement system is almost the same as the linear analysis value, while the result using the existing system with the load cell value with the dynamic jack mixed with the friction force is significantly different. Its maximum peak displacement of 25.7 mm is  $-60\%$  of the maximum



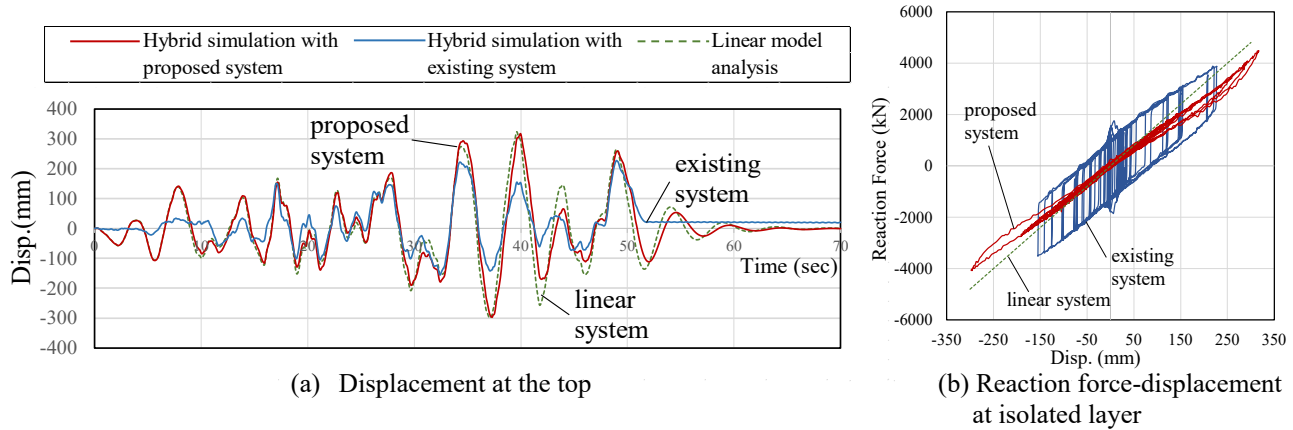


Fig. 27. Hybrid simulation result (Level 2 seismic motion).

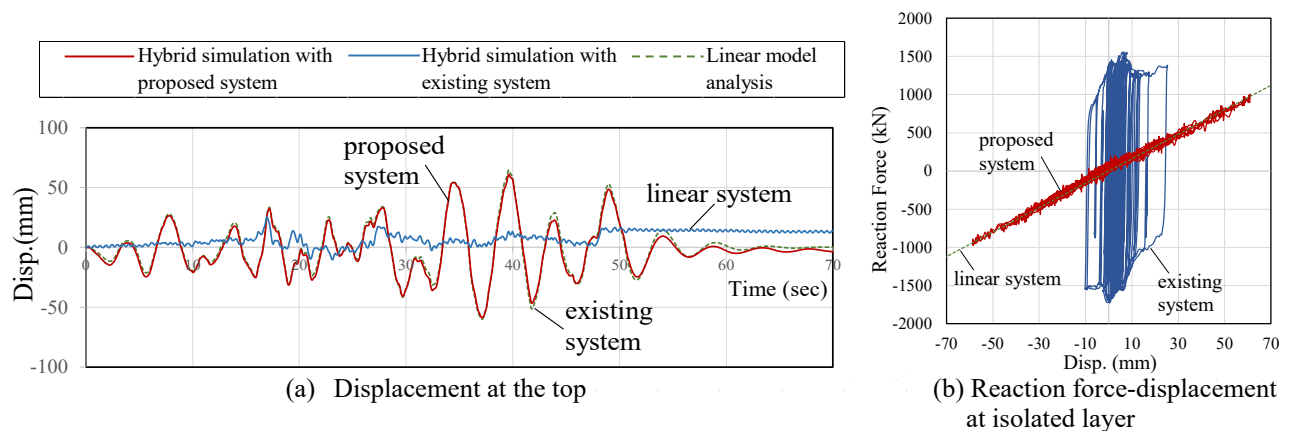


Fig. 28. Hybrid simulation result (Level 1 seismic motion).

value of the proposed system, whose errors are even larger than the level 2 ground motion. This means that the smaller the response amplitude, the larger the error due to the effect of friction force.

## 7. Conclusions

A method has been proposed to solve the problem of frictional and inertial forces mixing into the measured reaction force in dynamic test systems using a direct force measurement link that measures the reaction force on the reaction side separating horizontal and vertical reaction forces. In this paper, a scaled mockup test setup equipped with the proposed force measurement system was configured, and dynamic load tests were performed on the seismic isolation bearings, including a small-amplitude range. The obtained results are summarized as follows.

- 1) The proposed force measurement link was found to be effective through various dynamic conditions of vertical pressure and frequency with an error of less than 1%, whereas the conventional dynamic jack load cell measuring the reaction force was heavily affected by the inertial force under dynamic loading and frictional force when exposed to a vertical compression force.
- 2) A natural rubber based laminated rubber bearing showed linear shear force–displacement relationship and proved effective as an elastomeric isolator for supporting a reaction beam. However, it is desirable to adopt as rattle-free joints as possible for a measurement link to keep the force contribution ratio of the elastomeric isolator minimal, to eliminate the effects of their slight pressure dependency.

- 3) Dynamic experiments under high vertical pressure, excluding friction and inertial forces, revealed the precise dynamic characteristics and various dependencies of rubber seismic isolation bearings, including small amplifications that have been difficult to accurately evaluate.
- 4) Hybrid simulation tests using the proposed reaction force measurement system showed an overwhelming improvement in reproducibility of a physical experiment compared to conventional methods. This ability to accurately measure the specimen reaction force in real-time is expected to be a significant advantage for real-time hybrid simulations using this system in the future.

In the experiments conducted, the proposed force measurement system was also found to be effective in removing uneven friction errors due to the dent in the linear slider of this particular machine, which would have been difficult to remove with generalized friction models proposed in the past.

While the present study only covers the laminated rubber type bearing and focuses on the horizontal force measurement, the performance of the proposed system for the friction pendulum type bearing, which requires the control and precise measurement of the vertical force and the effects of high-frequency vibration of the reaction beam, should be further investigated.

## Declaration of Competing Interest

The authors declare the following financial interests/personal relationships which may be considered as potential competing interests:

T. Takeuchi et al.

Engineering Structures 296 (2023) 116844

Toru Takeuchi reports financial support was provided by Cross-ministerial Strategic Innovation Promotion Program (SIP), Japan.

#### Data availability

The authors do not have permission to share data.

#### Acknowledgements

This work was supported by the Council for Science, Technology, and Innovation (CSTI), Cross-ministerial Strategic Innovation Promotion Program (SIP), and Enhancement of National Resilience against Natural Disasters (Funding agency: National Institute for Earth Science and Disaster Resilience), Japan. We would like to thank Prof. Akira Wada, Prof. Shoichi Kishiki, Prof. Masako Yoneda and Prof. Kazuhiko Kasai of the Tokyo Institute of Technology, Mr. Yozo Shinozaki of Taisei Corporation and Dr. Fatih Sutcu of Istanbul Technical University for their excellent cooperation. The experiment was supported by the members of Takeuchi Laboratory at Tokyo Institute of Technology, and Takahashi Laboratory at Kyoto University, with valuable assistance received from Mr. Keita Ichihashi, Mr. Hiroki Ohmura, Mr. Ryota Tsudaha and Mr. Yuto Miyoshi. The SIP research project itself is supported by vast numbers of people which are listed in Ref. [7] (Takahashi et al. 2023).

#### References

- [1] Constantinou MC, Tsopelas P, Kasalanati A, Wolff ED. Property Modification Factors for Seismic Isolation Bearings. Technical Report MCEER-99-0012, University of Buffalo; 1999.
- [2] Constantinou MC, Whittaker AS, Kalpakidis Y, Fenz DM, Warn GP. Performance of seismic isolation hardware under service and seismic loading, Technical Report MCEER-07-0012, University of Buffalo; 2007.
- [3] Benzoni G, Seible F. Design of the Caltrans seismic response modification device (SRMD) test facility, Research co-ordination meeting of the IAEA's co-ordinated research programme on intercomparison of analysis methods for seismically isolated nuclear structures. 1998; 101–115 [https://inis.iaea.org/collection/NCLCollectionStore/\\_Public/31/047/31047660.pdf?r=1](https://inis.iaea.org/collection/NCLCollectionStore/_Public/31/047/31047660.pdf?r=1).
- [4] Lin TH, Chen PC, Lin KC. The multi-axial testing system for earthquake engineering researches. Earthq Struct 2017;13(2):165–76. <https://doi.org/10.12989/eas.2017.13.2.165>.
- [5] Alireza S, Schellenberg AH, Schoettler MJ, Mosqueda G, Mahin S. Real-time hybrid simulation of seismically isolated structure with full-scale bearings and large computational models. CMES 2019;120(3):693–717. <https://doi.org/10.32604/cmcs.2019.04846>.
- [6] Tsopelas P, Constantinou MC. Experimental Study of FPS System in Bridge Seismic Isolation. Earthq Eng Struct Dynam 1996;25:65–78.
- [7] Takahashi Y, Takeuchi T, Kishiki S, Yoneda M, Wada A. E-Isolation–High-performance dynamic testing installation for seismic isolation bearings and damping devices. Int J High-rise Build 2023;12(1):93–105.
- [8] Zayas V. Personal communication, EPS January 25, 2023; (<https://www.earthquakeprotection.com>).
- [9] Wada A, Kurosawa M, Tatsumi N, Kishiki S, Takeuchi T, Takahashi Y. Experiment of laminated rubber bearings under small deformation amplitudes. AIJ annual conference; 2022; 611-612 [In Japanese].
- [10] Takeuchi T, Kanda R, Ozaki H, Kitajima K. Design of seismic isolation and response-controlled structures. AIJ Kanto; 2007 [In Japanese].
- [11] Takahashi Y, Fenves GL. Fenves, Software framework for distributed experimental-computational simulation of structural systems. Earthq Eng Struct Dyn 2006;35(3): 267–91. <https://doi.org/10.1002/eqe.518>.
- [12] Schellenberg A, Kim HK, Takahashi Y, Fenves GL, Stephen A, Mahin SA. OpenFresco Command Language Manual (Ver.2.6), <available at <https://openfresco.berkeley.edu/>>. <https://openfresco.berkeley.edu/wp-content/uploads/2011/12/OpenFresco-Command-Language-Manual-2.6.pdf>.